On the Large-Eddy Simulations of the Flow Past a Cylinder at Critical Reynolds Numbers

O. Lehmkuhl, I. Rodríguez, J. Chiva and R. Borrell

1 Introduction

The flow past a circular cylinder is associated with different types of instabilities which involve the wake, the separated shear layers and the boundary layer. A comprehensive description of the flow phenomena at different Reynolds numbers (Re) can be found in [15]. It is well known that when the Reynolds number approaches 2×10^5 the boundary layer undergoes a transition from laminar to turbulent regime. The range of Reynolds numbers up to $\sim 3.5 \times 10^5$ is characterised by a rapid decrease of the drag coefficient with the Reynolds number. Another feature which characterises this regime is the presence of asymmetric forces during the transition regime as reported experimentally [2]. During this transition, the separation point moves towards the rear end of the cylinder until it reaches a stationary point with a stable drag coefficient. This marks the transition from the critical to the supercritical regime [11].

This work aims at shed some light into the complex physics present at these critical Reynolds numbers. To do this, large-eddy simulations of the flow at Reynolds numbers in the range of $Re = 1.4 \times 10^5$–5.3×10^5 are carried out. Solutions are compared to experimental measurements available in the literature. One of the

O. Lehmkuhl (✉) · I. Rodríguez · J. Chiva
Universitat Politècnica de Catalunya - BarcelonaTech, Colom 11,
08222 Terrassa, Spain
e-mail: oriol@cttc.upc.edu

I. Rodríguez
e-mail: ivette@cttc.upc.edu

J. Chiva
e-mail: jordic@cttc.upc.edu

R. Borrell
Termo Fluids S.L., Avda. Jacquard 97 1-E, 08222 Terrassa, Spain
e-mail: ricardb@cttc.upc.edu

J. Fröhlich et al. (eds.), *Direct and Large-Eddy Simulation IX*,
ERCOFTAC Series 20, DOI 10.1007/978-3-319-14448-1_36

major outcomes is to understand the physics that characterises the critical regime and the role of the turbulent transition in the boundary layer on the drag crisis phenomena.

2 Numerical Method

Large-eddy simulations (LES) of the flow are here performed. The methodology for solving the filtered Navier-Stokes equations is detailed in [8, 10]. As for the turbulence model, large-eddy simulations are carried out using the Wall-Adapting Local Eddy diffusivity model [9] within a Variational Multi-Scale framework (VMS-WALE subgrid-scale model) [6].

2.1 Definition of the Case: Geometry and Mesh Resolution

The flow past a circular cylinder at critical Reynolds numbers in the range of $Re = U_{ref}\ D/\nu = 1.4 \times 10^5$–$5.3 \times 10^5$ is considered. The Reynolds number is defined in terms of the free-stream velocity U_{ref} and the cylinder diameter D. The cases are solved in a computational domain of dimensions $x \equiv [-16D, 16D]$; $y \equiv [-10D, 10D]$; $z \equiv [0, 0.5\pi D]$ in the stream-, cross- and span-wise directions respectively, with a circular cylinder at (0, 0, 0). The boundary conditions at the inflow consist of uniform velocity (u,v,w) = (1, 0, 0), slip conditions at the top and bottom boundaries of the domain, while at the outlet a pressure-based condition is used. At the cylinder surface, no-slip conditions are prescribed. As for the span-wise direction, periodic boundary conditions are imposed.

The governing equations are discretised on an unstructured mesh generated by the constant-step extrusion of a two-dimensional unstructured grid. Different grids up to ∼64 million CVs are used, depending on the Reynolds number (see Table 1). The boundary layer at the cylinder surface is well resolved, i.e. no wall function is used. Thus, the meshes are designed so as to keep the non-dimensional wall distance $y^+ \leq 2$. To do this, a prism layer is constructed around the cylinder surface. In the problem here considered, transition to turbulence occurs in the boundary layer. Thus,

Table 1 Main parameters for the different computations

Re	NCV_t [MCVs]	$N_{CV\ plane}$	N_{planes}
1.44×10^5	38.4	299,683	128
2.6×10^5	38.4	299,683	128
3.8×10^5	48.6	379,950	128
5.3×10^5	64	500,516	128

NCV_t total number of CVs; $N_{CV\ plane}$ number of CVs in the plane; N_{planes} number of planes in the span-wise direction

it should be stressed that in the present formulation transition to turbulence is well captured by the model, i.e. no artificial mechanism is imposed for triggering this phenomenon to occur.

3 Results

For obtaining the numerical results presented, the simulations are started from an initially homogeneous flow field. Then, simulation is advanced in time until statistical stationary flow conditions are achieved and the initial transient is completely washed out. Average statistics are then computed for a sufficient long time span of about $\sim 100\, tU/D$, in order to assure that the flow is statistically converged.

In order to gain insight into the coherent structures developed in the separated zone, the Q-criterion is used [7]. Figure 1 shows the isocontours of second invariant of the velocity gradient tensor (Q) coloured by the velocity magnitude at Reynolds numbers of 2.5×10^5, 3.8×10^5 and 5.3×10^5. While the lower Reynolds number exhibits a flow topology more similar to that observed in the sub-critical regime, i.e. laminar flow

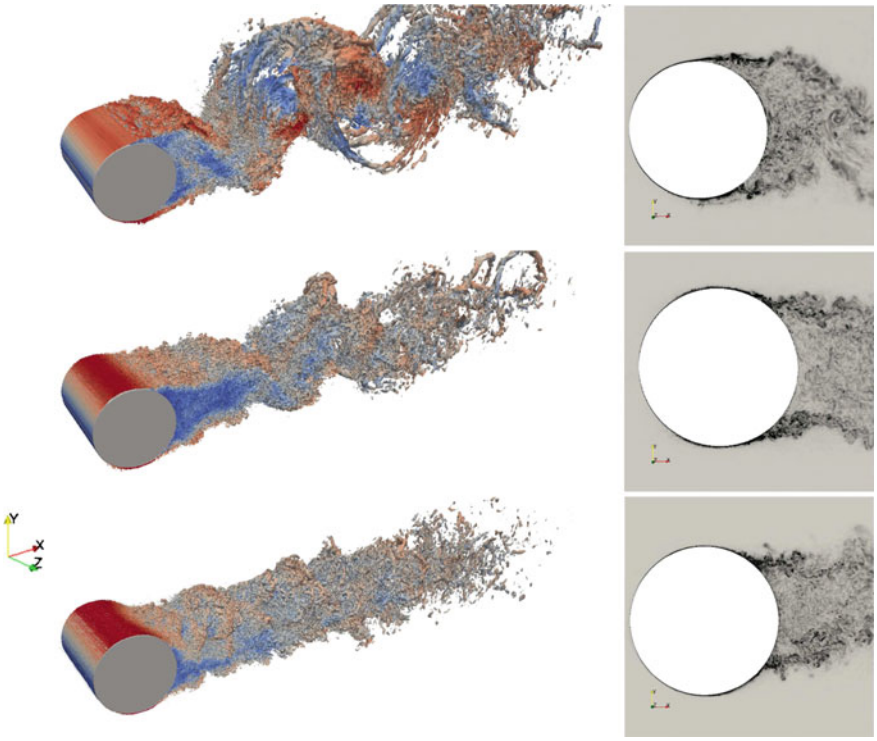

Fig. 1 Wake configuration. *Left* Q iso-countours coloured by the velocity magnitude; *right* instantaneous vorticity magnitude. From *top* to *bottom*: $Re = 2.6\times10^5$; $Re = 3.8\times10^5$; $Re = 5.3\times10^5$

separation at about ($\phi_s \sim 90°$) from the stagnation point and transition to turbulence in the separated shear layers, at the higher Reynolds numbers the flow shows a narrow wake with the separation point moving towards the rear end of the cylinder ($\phi_s \geq 90°$). The wake topology obtained at these critical Reynolds number can also be observed by means of the vorticity contours depicted at the half span-width plane.

Time-averaged statistical features resulting from the simulation are summarized in Table 2. In the table, the drag coefficient (C_D), the base pressure ($-Cp_b$), the separation angle measured from the stagnation point (φ_{sep}), and the angular position where the pressure reaches a minimum (φ_{Pmin}), are given. Experimental data from the literature are also given. As can be seen, in the range of Reynolds numbers considered, there is a pronounced decrease in the magnitude of the drag coefficient accompanied with an increase in the base pressure coefficient. As observed from the instantaneous flow, separation in the boundary layer is delayed, with increasing separation angle. The location of the pressure minimum also increases with the Reynolds number, moving towards the rear end of the cylinder, while its absolute value decreases (see also Fig. 2).

The variation of the drag coefficient with the Reynolds number is plotted in Fig. 2 together with reference data from the literature. At these Reynolds numbers, the measured data of the drag coefficient present a large scattering, due to the difficulties

Table 2 Statistical flow features at different Reynolds numbers

Re	C_D	$-Cp_b$	$\varphi_{sep}[°]$	$\varphi_{Pmin}[°]$
1.4×10^5	1.215	1.3	95.5	68.5
2.6×10^5	0.83	0.984	95/252	70/280
3.8×10^5	0.328	0.347	102	83.8
5.3×10^5	0.247	0.15	121	86
Cantwell and Coles Re = 1.4e5	1.237	1.21	–	–
Achenbach Re = 2.6e5	–	–	94	–

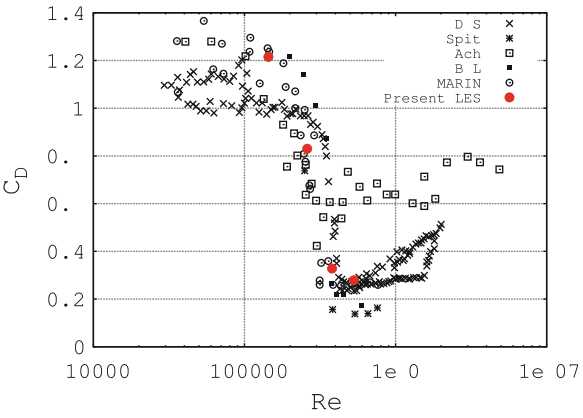

Fig. 2 Variation of the drag coefficient with the Reynolds number. Comparison with the literature. *Red circles* present results, *squares* Achenbach [1], *solid squares* Bursnall and Loftin [3], *stars* Spitzer [13], *crosses* Delany and Sorensen [5]., *circles* Vaz et al. [14]

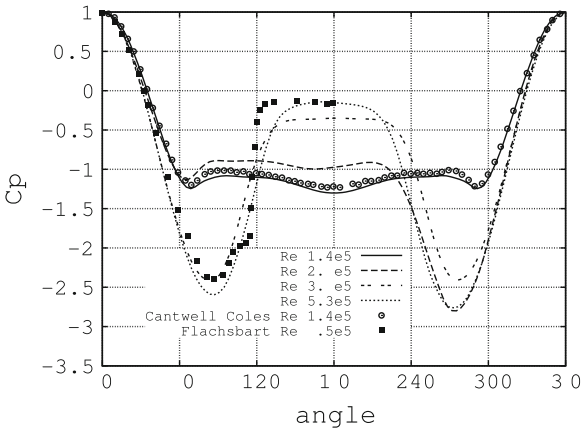

Fig. 3 Pressure distribution for the different Reynolds numbers

associated with the measurements; i.e. sensitiveness to turbulence intensity, cylinder end conditions, surface roughness, blockage ratio, etc. In spite of the large scattering in the reference data, results obtained with the present simulations show a fair agreement, being in the same range of the measured data.

In addition to the total drag coefficient, the pressure distribution at the cylinder surface at different Reynolds numbers is depicted in Fig. 3. As can be seen, at $Re = 1.44 \times 10^5$ it compares very well with that measured by Cantwell and Coles [4] at the same Reynolds number. As the Reynolds number increases, the pressure distribution changes with a pronounced decrease in the magnitude of the minimum pressure, and the position of this minimum moving towards the rear end of the cylinder. At the same time, the cylinder base pressure rises as was also shown by Achenbach [1] in his study. This behaviour is characteristic of the critical regime.

One interesting feature observed in the present computations is the presence of asymmetric forces at the cylinder surface in the regime transition (in the present computations at $Re = 2.5 \times 10^5$). Transition to turbulence occurs earlier at one side of the cylinder boundary layer. Thus, separation in the turbulent side is delayed. This behaviour, which causes large fluctuations in the cylinder forces and yields average lift $C_l > 0$, was also observed experimentally by Bearman [2] and Schewe [12]. As can be observed, at the $Re = 3.8 \times 10^5$ the forces at the cylinder recover their symmetry (see Fig. 3), whereas at $Re = 5.3 \times 10^5$ the drag coefficient reaches its minimum value (see also Fig. 2), but the pressure distribution is again slightly asymmetric.

4 Concluding Remarks

The flow past a circular cylinder at critical Reynolds numbers in the range of $Re = 1.4 \times 10^5$–5.3×10^5 is computed by means of large-eddy simulations. In the present computations, the mesh used is highly refined in the near-wall, as no wall

function is used for solving the turbulent boundary layers. Furthermore, it should also be stressed the capabilities of the current formulation for capturing quite well the transition to turbulence in the boundary layer without the use of any artificial mechanism which triggers this phenomenon to occur. Results shown are very promising as they correctly predict the steep drop in the drag coefficient in this range of Reynolds numbers and the delayed turbulent separation from the cylinder surface, being consistent with the experimental measurements. The presence of asymmetric forces on the cylinder surface occurring during the critical regime in agreement with previous experiments is also detected. It should be pointed out that in the present computations, these asymmetric forces are detected at the Reynolds number of 2.5×10^5, which is slightly earlier than in experimental measurements. The asymmetries in the pressure distribution should be interpreted as the starting point of the drag crisis, with the transition to turbulence occurring earlier at one side of the cylinder boundary layer, whereas the other side is still laminar. Thus, separation in the turbulent side is delayed. Last but not the least, mean pressure distributions on the cylinder surface are computed showing a reasonable agreement with previous experimental results.

Acknowledgments This work has been financially supported by the Ministerio de Economía y Competitividad, Secretaría de Estado de Investigación, Desarrollo e Innovación, Spain (Ref. ENE2010-17801) and, by the Collaboration Project between Universitat Politècnica de Catalunya and Termo Fluids S.L. We acknowledge PRACE for awarding us access to resource MareNostrum III based in Barcelona, Spain. We also acknowledge the technical expertise, assistance and access to MareNostrum II provided by the Red Española de Supercomputación.

References

1. Achenbach, E.: Distribution of local pressure and skin friction around a circular cylinder in cross-flow up to Re=5e6. J. Fluid Mech. **34**, 625–639 (1968)
2. Bearman, P.: On vortex shedding from a circular cylinder in the critical Reynolds number regime. J. Fluid Mech. **37**, 577–585 (1969)
3. Bursnall, W., Loftin L.J.: Experimental investigation of the pressure distribution about a yawed circular cylinder in the critical Reynolds number range. Technical report NACA TN2463, NACA (1951)
4. Cantwell, B., Coles, D.: An experimental study of entrainment and transport in the turbulent near wake of a circular cylinder. J. Fluid Mech. **136**, 321–374 (1983)
5. Delany, N., Sorensen, N.: Low-speed drag of cylinders of various shapes. Technical report NACA TN3038, NACA (1953)
6. Hughes, T., Mazzei, L., Jansen, K.: Large eddy simulation and the variational multiscale method. Comput. Vis. Sci. **3**, 47–59 (2000)
7. Hunt, J., Wray, A., Moin, P.: Eddies, stream and convergence zones in turbulent flows. Technical report CTR-S88, Center for Turbulent Research (1988)
8. Lehmkuhl, O., Rodríguez, I., Baez, A., Oliva, A., Pérez-Segarra, C.: On the large-eddy simulations for the flow around aerodynamic profiles using unstructured grids. Comput. Fluids **84**, 176–189 (2013)
9. Nicoud, F., Ducros, F.: Subgrid-scale stress modelling based on the square of the velocity gradient tensor. Flow Turbul. Combust. **62**, 183–200 (1999)
10. Rodríguez, I., Borrell, R., Lehmkuhl, O., Pérez-Segarra, C., Oliva, A.: Direct numerical simulation of the flow over a sphere at Re = 3700. J. Fluid Mech. **679**, 263–287 (2011)

11. Roshko, A.: Experiments on the flow past a circular cylinder at very high Reynolds number. J. Fluid Mech. **10**(03), 345–356 (1961)
12. Schewe, G.: On the force fluctuations acting on a circular cylinder in crossflow from subcritical up to transcritical Reynolds numbers. J. Fluid Mech. **133**, 265–285 (1983)
13. Spitzer, R.: Measurements of unsteady pressures and wake fluctuations for flow over a cylinder at supercritical Reynolds number. Ph.D. thesis, California Institute of Technology (1964)
14. Vaz, G., Mabilat, C., van der Wal, R., Gallagher, P.: Viscous flow computations on a smooth cylinders: a detailed numerical study with validation. In: Proceedings of 26th International Conference on Offshore Mechanics and Arctic Engineering. OMAE2007, San Diego, California (2007)
15. Williamson, C.H.K.: Vortex dynamics in the cylinder wake. Annu. Rev. Fluid Mech. **28**(1), 477–539 (1996)